Results in Surfaces and Interfaces 9 (2022) 100089

Contents lists available at ScienceDirect

Results in Surfaces and Interfaces

journal homepage: www.elsevier.com/locate/rsurfi

The influence of the electrolytic bath on the hard anodizing of diecast Al–Si–Cu alloys

Giulia Scampone [a,*], Antonio Russo [b], Alessio Carminati [c], Giulio Timelli [a]

[a] Department of Management and Engineering, University of Padova, Stradella S. Nicola, 3, 36100 Vicenza, Italy
[b] Alfa Ossidazione – Gaser group, Via Dott. Raffaele De Troya, 65/67, 25010 Borgosatollo (BS), Italy
[c] Gaser Ossido Duro– Gaser group, Via Po, 27, 20089 Rozzano (MI), Italy

ARTICLE INFO

Keywords:
Anodizing
AlSiCu alloys
Electrolyte
Microstructure
Wear
Surface mechanical properties

ABSTRACT

In the present work, the influence of the temperature and concentration of the electrolyte on the anodizing response of a high-pressure diecast AlSi11Cu2(Fe) alloy was studied. Sandblasted components, produced by high pressure diecasting, were anodized at −4.5 °C or +5 °C in an electrolyte with a free sulfuric acid concentration of 168 g/L or 217 g/L. Metallographic and image analysis techniques were carried out to study the changes in the oxide layer in terms of thickness and morphology. Scratch and wear tests were also performed to characterize the surface mechanical properties. The results show how the thickness of the anodic layer can be increased by decreasing the anodizing temperature of the electrolytic bath otherwise increasing the concentration of the sulfuric acid. However, the combination of a low anodizing temperature and a high concentration of free sulfuric acid has no beneficial effect on the formation of the anodic film. In this condition, the dissolution phenomena of the oxide layer inside the electrolyte are promoted and a thinner low-performance anodic layer is formed. Finally, the wear and scratch resistance are maximized after anodizing at −4.5 °C in an electrolyte with a concentration of sulfuric acid equal to 168 g/L.

1. Introduction

In high pressure diecasting, Al–Si–Cu alloys are one of the most widely used groups among the Al foundry alloys due to their great castability and the good mechanical properties, especially after heat treatment (Mohamed and Samuel, 2012). These alloys are mainly employed in the automotive sector, where the production of lightweight, high-performance and electrically insulating components is required. In order to improve the surface hardness, electrical insulation, wear and corrosion resistance of the casting, an anodizing treatment can be performed (Runge, 2018). During this electrochemical treatment, the Al surface is the anode of the electrolytic cell and the growth of aluminum oxide is artificially induced on the metal substrate through the action of electrical current (ASM HandBook, 1994; Scampone and Timelli, 2022).

In the MIL-A8625 specification, several types of anodizing are identified according to process temperature and type of electrolyte. Among them, hard anodizing is the most suitable treatment to maximize the abrasion resistance and the hardness of the oxide layer. This treatment is performed in a sulfuric acid electrolyte at a temperature lower than 10 °C (MIL-A-8625F, 1993).

The growth of the oxide film is based on an ion exchange between the Al substrate and the electrolyte (Runge, 2018; Stojadinović et al., 2014). Under the influence of an high electric field, the anions contained in the sulfuric acid electrolyte (O^{2-}, OH^{-}, SO_4^{2-}) migrates towards the Al casting and they react with the aluminum cations (Al^{3+}) formed from the dissolution of the aluminum substrate. This reaction results in the formation of aluminum oxide (Al_2O_3) at the metal/oxide and oxide/electrolyte interfaces. However, at the oxide/electrolyte interface, the Al_2O_3 can also dissolve inside the electrolyte, allowing the formation of a porous structure (Stojadinović et al., 2014). Therefore, the anodic layer grows until a balance is reached between the formation rate of Al_2O_3 and its dissolution rate in the electrolyte.

The temperature and the concentration of the electrolytic bath strongly influence the thickness and the performance of the anodic layer. Low concentrations of H_2SO_4 mitigate the formation of cracks in the oxide layer (Chung et al., 2017, 2018), improving the surface microhardness and abrasion resistance (Gastón-García et al., 2011). Furthermore, upon reducing the temperature of the electrolyte, its reactivity decreases, and a thicker anodic layer is formed, due to the lower dissolution rate (Gastón-García et al., 2011). However, at lower electrolytic temperatures, the resistance of the electrolyte to the current flow increases, reducing the anodizing efficiency (Vinal and Craig, 1934). Caliari (2017) reported that lowering the bath temperature from 0 °C to −4 °C leads to thinner oxide films; the increase in electrolyte

* Corresponding author.
E-mail addresses: giulia.scampone@phd.unipd.it (G. Scampone), antonio.russo@gruppogaser.com (A. Russo), alessio.carminati@gruppogaser.com (A. Carminati), timelli@gest.unipd.it (G. Timelli).

https://doi.org/10.1016/j.rsurfi.2022.100089
Received 31 July 2022; Received in revised form 19 October 2022; Accepted 21 October 2022

Table 1
Chemical composition of the diecast alloy (wt.%).

Al	Si	Fe	Cu	Mn	Mg	Zn	Cr	Ti	Ni
bal.	11.5	1.1	1.8	0.55	0.30	1.70	0.15	0.25	0.45

resistance limits the coarsening of the anodic layer by prevailing over the reduction of Al_2O_3 dissolution rate.

In general, at lower anodizing temperature, a denser and high-performance anodic layer with less porosities is formed due to the reduction of the local heating effects on the oxide surface (Aerts et al., 2007; Niyazbakhsh et al., 2019). However, the diffusion velocity of reactants is also reduced, and voids can be formed inside the anodic structure if the gaseous products are not totally removed from the reacting interphase during anodizing (Bononi et al., 2017).

Most of the studies focused on anodizing were carried out on pure aluminum or wrought Al alloys, because due to the high amount of alloying elements, foundry Al alloys are difficult to anodize (Scampone and Timelli, 2022). However, the current focus on environmental sustainability and the spread of electric cars, which require electrically insulated components, have made it essential to extend the anodizing process to Al foundry alloys as well. Therefore, the aim of this study is to compensate this lack of knowledge by investigating the influence of the temperature and concentration of the electrolyte on the anodizing behavior of a high-pressure diecast AlSi11Cu2(Fe) alloy.

2. Experimental procedure

2.1. Casting and anodizing parameters

An high pressure diecast component, produced with a standard AlSi11Cu2(Fe) alloy (EN AC-46100, BS EN 1706, 2020), was selected for the analysis. The castings for the experimental trials were produced using a cold chamber die-casting machine, setting a casting temperature of 680 ± 5 °C. Samples for the analysis of the chemical composition were poured separately and analyzed by optical emission spectrometry (Table 1).

Before anodizing, the castings were sandblasted and treated in a water solution of neutral liquid degreaser Alucleaner 18 (Aluservice, 2012). After rising in deionized water, hard anodizing was performed under galvanostatic conditions in a sulfuric acid electrolyte. In general, hard anodizing is industrially performed at a temperature between −5 and +5 °C (Henley, 1982), with a free sulfuric acid concentration ranging from 165 to 225 g/L (Poyner, 1991). To study the effect of these process parameters on the anodizing response, each parameter was varied over two levels close to the extremes of the industrial ranges. Therefore, the concentration of free H_2SO_4 in the electrolyte was equal to 168 or 217 g/L; on the other side, due to plant limitations, the anodizing temperature was set at −4.5 or +5 °C. Moreover, the DC electric current density was first linearly increased from 0 to 0.88 A/dm^2 in 20 min, and then kept constant at 0.88 A/dm^2 for 35 min, according to industrial practice (Henley, 1982). Finally, the castings were sealed for 10 min in a water solution of NiF_2 at 25 ± 2 °C.

Samples for microstructural analysis, wear and scratch tests were drawn from the same region of different castings.

2.2. Microstructural characterization

An optical microscope and a field-emission gun scanning electron microscope (FEG-SEM) equipped with energy dispersive spectrometer (EDS) were used for the microstructural investigations. Both untreated and anodized samples were traditionally grinded and polished with 3 μm diamond paste and 0.04 μm silica colloidal suspension.

The untreated substrate was firstly investigated. At least 10 contiguous micrographs, each with an area of 240 × 170 μm^2, were collected along the casting surface. The area fractions of Fe- and Cu rich compounds were quantified by using an image analyzer software. To simplify the identification of Fe-rich particles, the polished specimens were etched in a water solution of 20% H_2SO_4, heated at 70 °C. Instead, an aqueous solution of 25% HNO_3 at 70 °C was used to analyze Cu-rich compounds. The eutectic fraction was also quantified after chemical etching in a modified Murakami solution (60 mL H_2O, 10 g NaOH, and 5 g $K_3Fe(CN)_6$). Moreover more than 500 Si eutectic particles were analyzed to study their average size, defined as the equivalent circle diameter.

The line intercept method (Vandersluis and Ravindran, 2017) and EN ISO 1463:2004 standard were used to measure the secondary dendrite arms spacing (SDAS) and the thickness of the oxide layer, respectively.

Some anodized samples were prepared by freeze-fracture technique (Kuo, 2014) to investigate the morphology of the oxide film cross-section.

Finally, the average surface roughness (Ra) was measured by using a Taylor Hobson Surtronic 3+ stylus profilometer, with a resolution of 0.01 μm.

2.3. Wear and scratch tests

Ball-on-disc wear tests were performed at 25 ± 5 °C and 10%–15% of relative humidity, using a 6-mm-diameter Al_2O_3 sphere as counter body. A distance of 163 m, with a sliding speed of 0.06 m/s, and an applied load of 2 N were selected as conditions for the dry sliding tests. Each test lasted about 45 min and at least 3 tests were performed for each condition.

The wear rate (ω) was calculated as

$$\omega = \frac{V}{L \cdot N} \quad (1)$$

where V is the volume of material worn out during the test, L is the sliding distance and N is the applied load.

A stylus profilometer was used to measure both the profile and the area of the wear track after each test. The wear volume (V) was determined as the average wear area integrated over the perimeter (p) of the circular wear track ($p = 2 \cdot \pi \cdot r$, with r = 5.2 mm).

During the trials, both the oxide layer and the substrate wore out. Therefore, the wear resistance of the "oxide film + aluminum alloy substrate" system was analyzed.

The scratch resistance was evaluated according to the BS EN ISO 22557 (2020), by using an Erichsen Hardness Test Pencil (Model 318). The tests were performed at room temperature and the critical load was determined by applying increasing load until the oxide layer was scratched and the substrate exposed.

3. Results and discussion

3.1. Microstructure of the substrate

The microstructure of the investigated alloy is shown in Fig. 1. It consists mainly of primary α-Al dendrites and Al–Si eutectic structure. The high-pressure diecasting process is characterize by high cooling rates, which lead to the formation of an equiaxed and less-branched dendrites α-Al phase and a refined eutectic structure. The eutectic Si particles show a fibrous and fine morphology with an average size of 0.3 ± 0.1 μm. Fe-rich compounds are also present in the form of blocky-like α-$Al_x(Fe,Mn,Cr)_ySi_z$ particles (Fig. 1) and they occupy an area fraction of 3.6 ± 0.6%.

Table 2 reports the chemical composition of the investigated substrate, measured by optical emission spectrometry. Although 1.64 wt.% Cu was measured, no Cu-rich particles were detected in the microstructure. This result is reasonably caused by the high cooling rate, which prevented the precipitation of Cu-rich compounds and led to the Cu retainment in solid solution within the α-Al matrix. Moreover, Table 2 shows a higher Si content if compared to the chemical composition

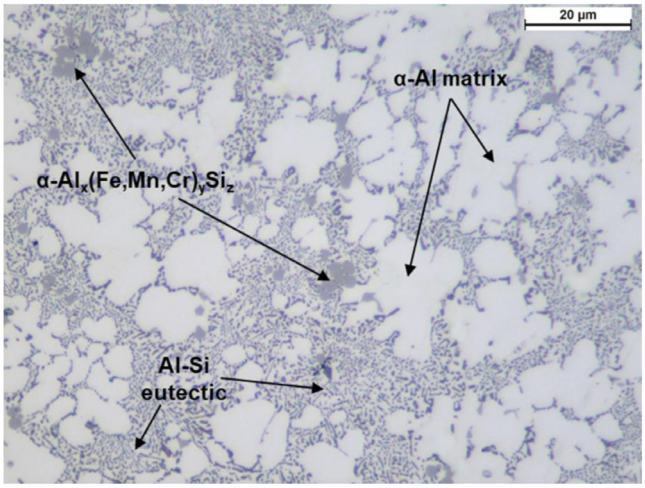

Fig. 1. Micrograph of the diecast AlSi11Cu2(Fe) alloy.

Table 2
Chemical composition (wt.%) of the investigated surface substrate.

Al	Si	Fe	Cu	Mn	Mg	Zn	Cr	Ti	Ni
bal.	12.8	1.1	1.6	0.26	0.09	1.07	0.10	0.04	0.06

reported in Table 1. The reason of this discrepancy lies in the positive macrosegregation that Al–Si diecastings usually exhibit on the casting surface. Timelli and Fabrizi (2014) showed that higher solute content form during solidification on the casting surface than in the underlying zone due to the combined effect of inverse segregation and exudation phenomena. Since the investigated area is located on the casting surface, the Si concentration is greater than the nominal value reported in Table 1, and the measured eutectic fraction results 60±5%.

3.2. Microstructure of the anodic layer

Fig. 2 shows the typical anodic layer grown on the AlSi11Cu2(Fe) substrate. A thin and compact oxide film formed on the casting surface. The EDS mapping shows that the eutectic Si particles are entirely embedded inside the anodic film and they are only partially oxidized (Fig. 2). When the oxidation front reaches a Si particle, a thin film of SiO_2 is formed on the particle surface.

The further oxidation of the Si phase would require more energy than the oxidation of the surrounding Al matrix, so the oxidation front continues to grow circumventing the particle (Scampone and Timelli, 2022; Fratila-Apachitei et al., 2004). Si particles are therefore incorporated inside the oxide layer and, according to their size and morphology, they can interrupt the continuity of the anodic film, forming a scalloped substrate/oxide interface (Fratila-Apachitei et al., 2004; Zhu et al., 2019). In the present work, the size of the eutectic Si particles is generally smaller than 5 µm, thus not deleterious for the uniform growth of the anodic layer (Fratila-Apachitei et al., 2004).

During anodizing, the oxidation front also interacts with the blocky-like α-Al$_x$(Fe,Mn,Cr)$_y$Si$_z$ compounds. In general, iron-rich intermetallics exhibit a different oxidation energy than the surrounding Al-matrix and they can hinder the growth of the anodic layer, generating a scalloped substrate/oxide interface (Mukhopadhyay and Sharma, 1997). Furthermore, they can be partially or totally dissolved, leading to the formation of voids or defects inside the anodic layer (Zhu and Zanella, 2021). The EDS mapping in Fig. 2 confirms the dissolution of α-Al$_x$(Fe,Mn,Cr)$_y$Si$_z$ compounds within the anodic layer; the presence of Fe and Mn fades drastically in the areas of the particle traversed by the oxidizing front. The mapping shows also the presence of S within the anodic film. This is due to the migration of SO_4^{2-} ions from the electrolyte to the metal/oxide interface and their subsequent incorporation in the anodic layer during the anodizing process (Runge, 2018).

Figs. 3 and 4 show the influence of different anodizing parameters on the growth of the anodic layer. When the electrolytic bath had a temperature of +5 °C and a free sulfuric acid concentration of 168 g/L, the thickness of the oxide film was 3.4 ± 1.2 µm (Fig. 3a). Upon decreasing the temperature to −4.5 °C and keeping constant the concentration of H_2SO_4, the thickness increased to 5.5 ± 1.6 µm (Fig. 3b), due to the lower dissolution rate of Al_2O_3 in the electrolyte (Runge, 2018; Gastón-García et al., 2011).

In addition, the increase of free sulfuric acid concentration to 217 g/L at the temperature of +5 °C promoted the growth of the anodic layer. This last increased from 3.4 ± 1.2 µm to 5.2 ± 2.1 µm (Fig. 3c), due to the greater reactivity of the electrolyte. However, when the temperature of the electrolyte was low (−4.5 °C) and the H_2SO_4 concentration was high (217 g/L), the anodic layer resulted thinner (4.6 ± 1.5 µm). This result was related to the combined effect of the low anodizing temperature and the high concentration of free sulfuric acid. Low temperatures decrease the oxide dissolution rate but enhance the resistance of the electrolyte to the current flow (Vinal and Craig, 1934). On the other hand, high concentrations of free sulfuric acid increase both the conductivity and the aggressiveness of the electrolyte (Poznyak et al., 2021). The interaction between these aspects determine the final thickness of the anodic layer, whose growth is based on the balance between the formation and the dissolution rates of alumina in the electrolyte. At −4.5 °C with 217 g/L of H_2SO_4, the increase of the resistance of the electrolyte to the current flow prevails over the reduction of Al_2O_3 dissolution rate, resulting in a thinner anodic layer.

Fig. 5 shows the trend of the surface roughness by varying the anodizing conditions. Before anodizing, the substrate had a mean Ra value of about 5.1 µm, in agreement with the typical values of surface finish after the sandblasting process (Finger et al., 2020). After anodizing, the average surface roughness slightly increased to about 5.6 µm. No significant influence of the anodizing temperature or free sulfuric acid concentration was found.

3.3. Scratch results

Fig. 6 shows the influence of different anodizing conditions on the scratch resistance of the anodic layer. The adhesion of the oxide film was quantified in term of critical load, i.e. the force required to scratch the anodic layer and reveal the substrate.

The worst performance was obtained after anodizing at −4.5 °C with a free sulfuric acid concentration of 217 g/L, where the critical load was equal to 2.5 ± 1 N. These anodizing parameters were also found to be particularly unfavorable to the growth of the oxide layer (Fig. 4), as they favored the dissolution of the oxide layer rather than its growth (see Section 3.2). The low value of the critical load was therefore caused by the strong dissolution effects on the outer region of the anodic layer, which decreased the oxide microhardness (Fratila-Apachitei et al., 2003) and thus its scratch resistance. No significant differences in scratch resistance were observed in the anodic layer formed with the other conditions, where the critical load was about 5 ± 1 N.

3.4. Wear behavior

The variation of wear rate as a function of the mean thickness of the anodic layer is illustrated in Fig. 7. The wear rate was calculated as indicated in Eq. (1) (see Section 2.3), so higher values of this parameter correspond to lower wear resistance. As expected, after anodizing, the wear resistance increased regardless of the anodizing parameters, due to the formation of the anodic layer which showed higher surface hardness than the un-treated substrate (Runge, 2018). In general, an increase in the thickness of the anodic layer corresponds

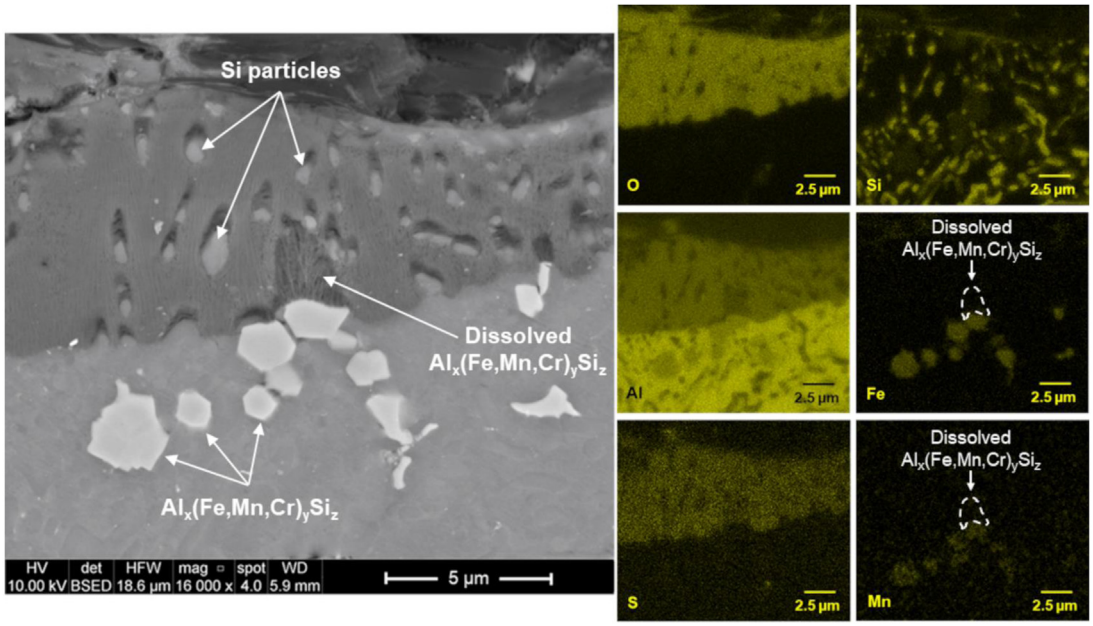

Fig. 2. FEG-SEM micrograph and EDS mapping showing the typical anodic layer formed on the diecast AlSi11Cu2(Fe) alloy. The micrograph refers to the sample anodized at −4.5 °C, with 168 g/L of free sulfuric acid in the electrolyte.

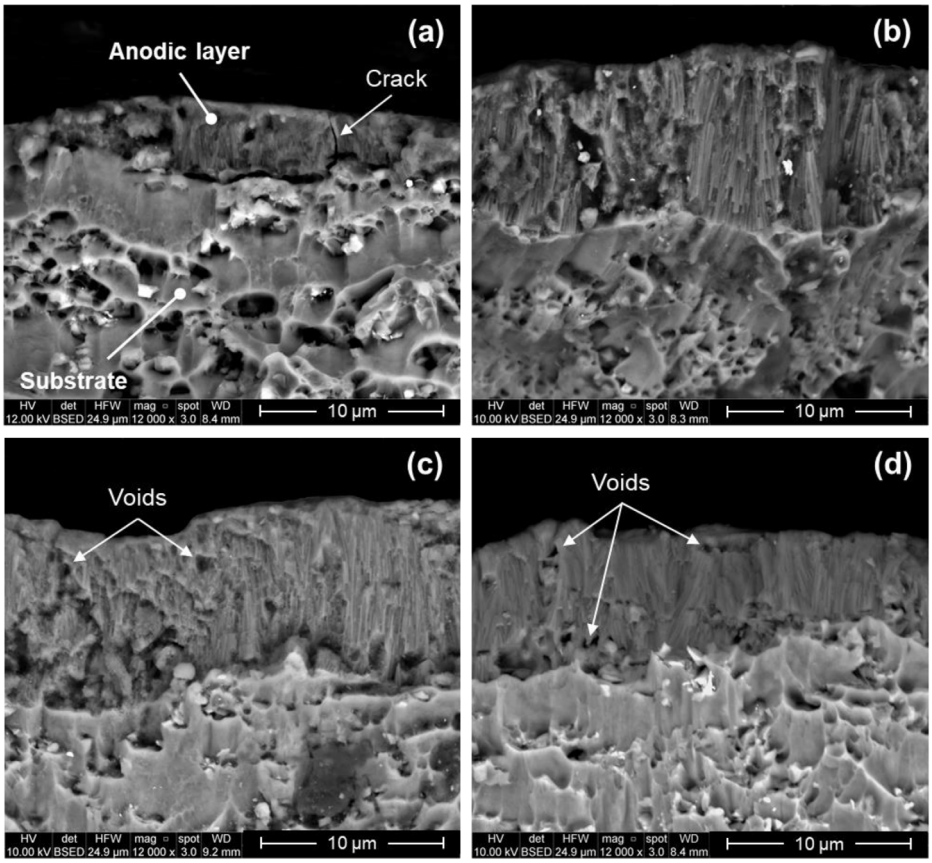

Fig. 3. FEG-SEM micrographs of the fractured cross-section of the anodized samples treated at different anodizing conditions: (a) +5 °C and 168 g/L H_2SO_4, (b) −4.5 °C and 168 g/L H_2SO_4, (c) +5 °C and 217 g/L H_2SO_4 and (d) −4.5 °C and 217 g/L H_2SO_4.

to a reduction in the wear rate. The optimal wear resistance within the investigated process conditions was obtained after anodizing at −4.5 °C with a free sulfuric acid concentration of 168 g/L H_2SO_4, when a thicker and high-performing oxide film was formed. When the anodizing temperature is low, the effects of the local heating on the oxide surface are reduced, and an anodic layer with less porosity is

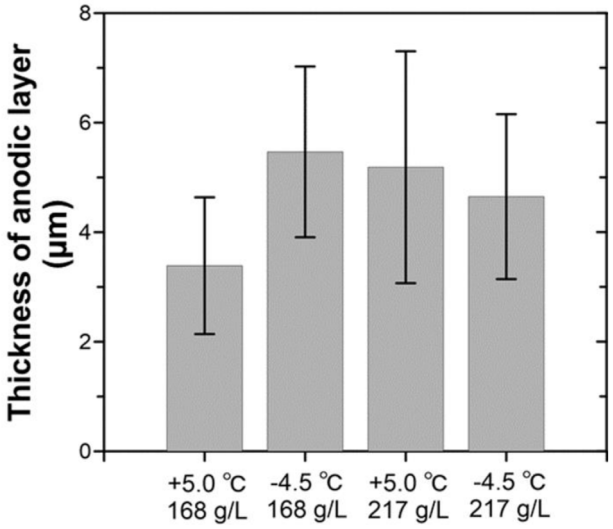

Fig. 4. Thickness of the anodic layer formed at different temperatures and H_2SO_4 concentrations of the electrolytic bath.

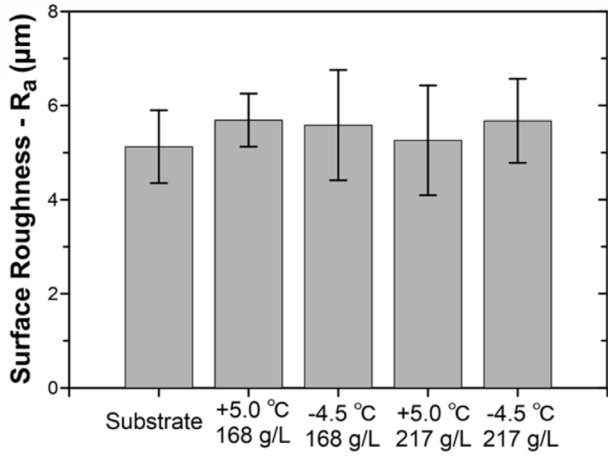

Fig. 5. Surface roughness of both the substrate and anodic layer at the different experimental conditions.

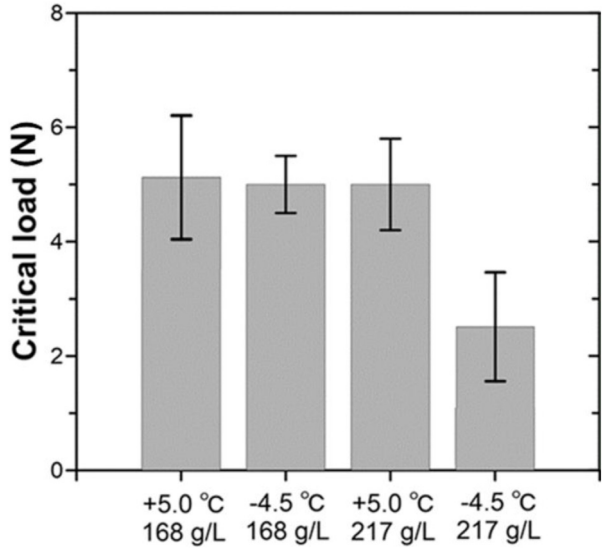

Fig. 6. Scratch resistance of the oxide layer formed at different temperatures and free sulfuric acid concentrations. The critical load corresponds to the force required to scratch the oxide layer and expose the substrate (ISO 22557:2020).

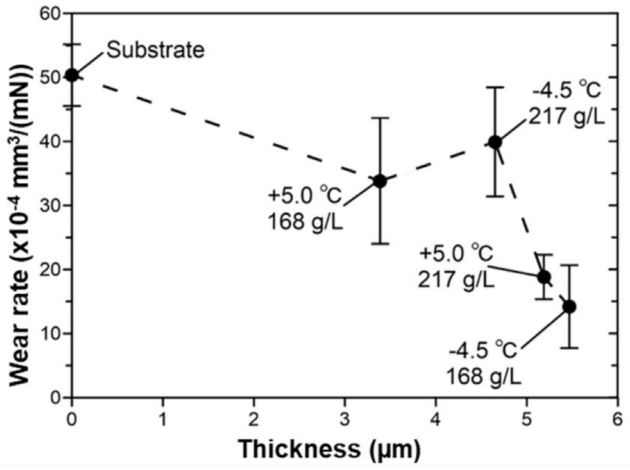

Fig. 7. Wear rate as a function of the thickness of the anodic layer. The labels indicate the anodizing conditions (i.e. temperature and free sulfuric acid concentration).

usually formed (Aerts et al., 2007). Moreover, lower concentrations of H_2SO_4 improve the mechanical properties of the oxide film. Gastón-García et al. (2011) demonstrated as anodic layers formed at lower concentration of sulfuric acid presented less cracks and defects, which resulted in higher microhardness and abrasion resistance.

The samples anodized at −4.5 °C with a free sulfuric acid concentration of 217 g/L showed greater wear rate than samples with thinner anodic layer. Therefore, it can be deduced that at −4.5 °C with 217 g/L of free H_2SO_4, a low-performing oxide film was formed. This result is in line with the findings reported in Section 3.3, where the samples treated under these conditions showed the worst scratch resistance. Moreover, in Section 3.2 it has already been discussed how these anodizing conditions promoted the dissolution of the outer region of oxide layer in the electrolyte, causing a decrease in surface microhardness and wear resistance (Fratila-Apachitei et al., 2003).

Fig. 8 shows the wear track formed over the anodized surface in the best (−4.5 °C, 168 g/L H_2SO_4) and worst (−4.5 °C, 217 g/L H_2SO_4) experimental conditions. The wear track obtained with higher concentration of H_2SO_4 was wider if compared to the track formed with a concentration of 168 g/L H_2SO_4. These findings are consistent with the wear rate trend illustrated in Fig. 7. The wear rate measured on the sample anodized at −4.5 °C and 217 g/L of free sulfuric acid was greater than the one measured on the sample anodized at −4.5 °C and 168 g/L H_2SO_4.

The main wear mechanism was adhesive wear. Marks of plastic deformation were observed in both the worn surfaces, even if they were more evident in the sample anodized with a higher free sulfuric acid concentration. In that sample, visible ploughing marks were also detected in the wear tracks (Fig. 8d), indicating that abrasive wear also occurred as secondary wear mechanism. Tiny fragments of abraded material can be observed in Fig. 8c and d. These fragments play a key role in the abrasive wear, because when they remain entrapped between the counter body and the sample, three-body abrasion phenomena takes place and deep abrasion marks form inside the wear track. After all the tests, the counter body did not show signs of abrasion, but only adhesion phenomena of debris of aluminum or alumina on its surface.

Fig. 9 shows the variation of the friction coefficient over the sliding distance in un-treated and anodized surfaces. Similar evolutions of the friction coefficient were observed in the anodized surfaces regardless of the anodizing parameters. In both un-treated and anodized conditions, the friction coefficient showed an initial run-in and a subsequent steady state. In the first phase, the Al_2O_3 ball entered in contact with the sample and started to abrade the surface. The abraded debris was transferred from the sample surface to the counter body, gradually covering

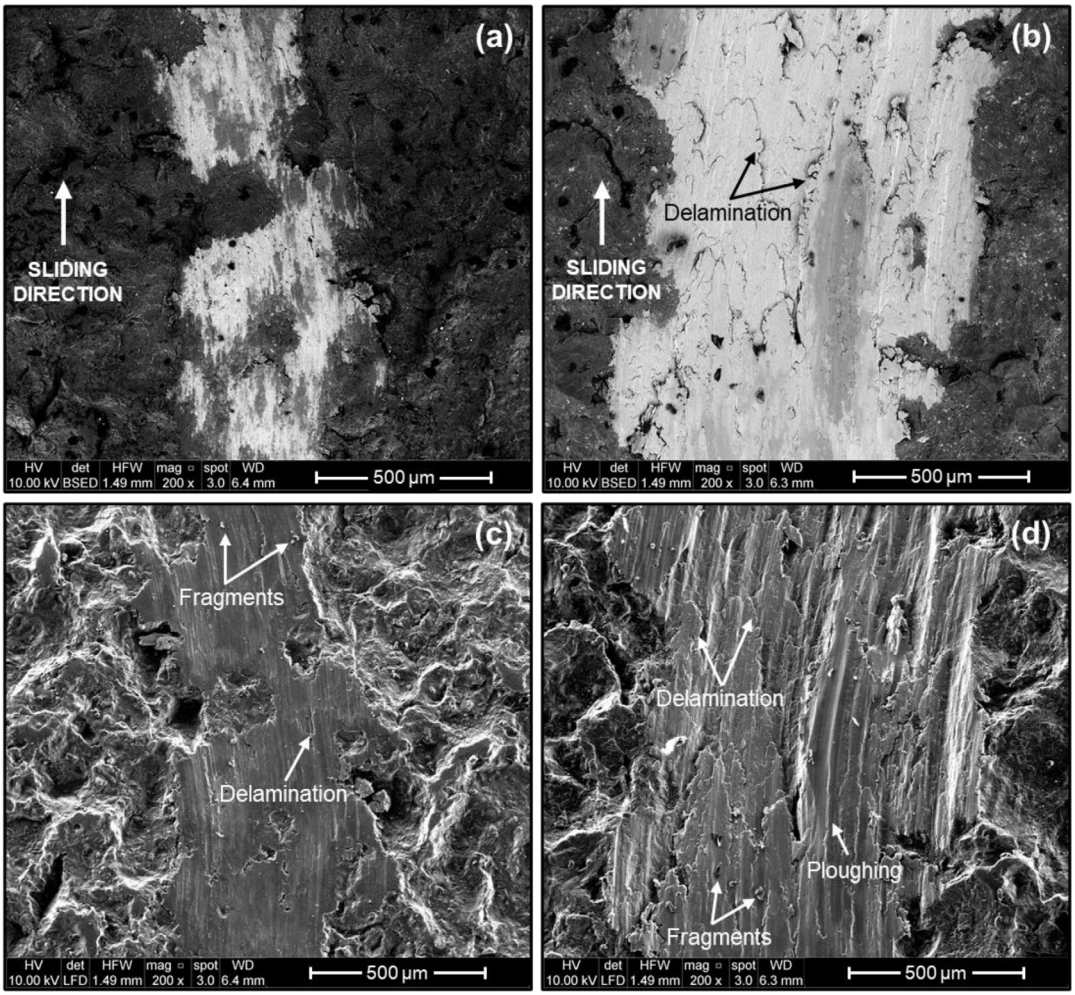

Fig. 8. FEG-SEM micrographs of the wear tracks of the sandblasted AlSi11Cu2(Fe) alloy surfaces after anodizing at (a, c) −4.5 °C and 168 g/L H_2SO_4 and (b, d) −4.5 °C and 217 g/L H_2SO_4. The micrographs (a, b) were acquired with the backscattered electron detector, while (c, d) with the secondary electron detector.

surface of the Al_2O_3 sphere. In the un-anodized sample the friction coefficient rapidly grew to 0.7, due to the initial contact between the Al_2O_3 ball and the Al substrates. As the sliding distance increased, the debris of the alloy substrate was easily transferred to the counter body, due to the high plasticity of the α-Al matrix, and the value of the friction coefficient gradually decreased to 0.4. On the other side, the friction coefficient progressively increased from 0.15 to 0.4 without any initial peak in the anodized surfaces. In this case, the Al_2O_3 sphere first entered in contact and worn the anodic layer, resulting in low values of the friction coefficient. Then, as the sliding distance increased, a greater amount of substrate was revealed and worn, resulting in the gradually increase of the friction coefficient. In the steady-state condition, the surface of the counter body was covered by a layer of transferring debris, and the values of the friction coefficient stabilized around 0.4–0.45 for both un-treated and anodized samples.

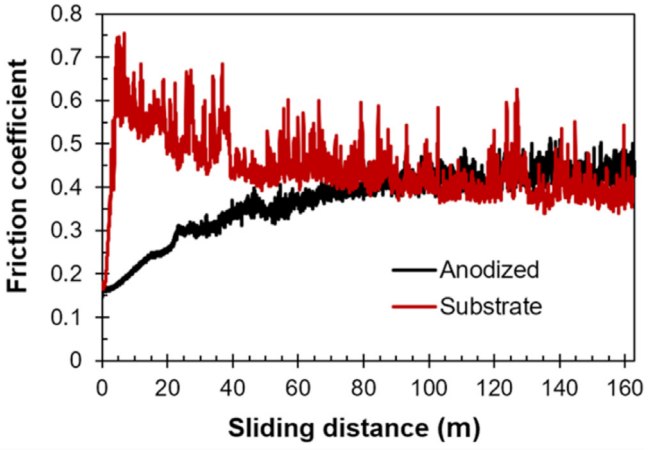

Fig. 9. Evolution of the friction coefficients of the substrate and the anodized surfaces as function of the sliding distance during the wear tests.

4. Conclusions

In the present work, the influence of the sulfuric acid electrolyte on the anodizing response of a diecast AlSi11Cu2(Fe) alloy was investigated. The functional properties of the anodic layer formed at different anodizing temperatures and free H_2SO_4 concentrations were analyzed in details. The following conclusions can be drawn:

- A thick oxide layer is formed when the anodizing temperature and the free sulfuric acid concentration are well balanced. An increase in the thickness of the anodic layer can be obtained at low anodizing temperature or at high concentration of free sulfuric acid.
- The combination of low anodizing temperatures and high concentrations of free sulfuric acid does not lead to the formation of a thick and high-performance oxide layer. The electrolyte exhibits a higher resistance to current flow, which, combined with

dissolution phenomena, does not favor the growth of the anodic layer and promotes its dissolution in the electrolyte.
- The surface roughness slightly increases after the anodizing process but it is not particularly affected by the anodizing temperature or free sulfuric acid concentration.
- The anodizing process increases the wear resistance of the diecast AlSi11Cu2(Fe) alloy, especially when a thicker and cracks-free anodic layer is formed.

Declaration of competing interest

The authors declare that they have no known competing financial interests or personal relationships that could have appeared to influence the work reported in this paper.

Data availability

Data will be made available on request.

Acknowledgments

The work was developed with the financial support of Fondazione Cassa di Risparmio di Padova e Rovigo (CaRiPaRo), Italy.

Ethics approval

This article does not contain any studies with human participants or animals performed by any of the authors.

References

Aerts, T., Dimogerontakis, T., de Graeve, I., Fransaer, J., Terryn, H., 2007. Influence of the anodizing temperature on the porosity and the mechanical properties of the porous anodic oxide film. Surface and Coatings Technology 201 (16–17), 7310–7317. http://dx.doi.org/10.1016/j.surfcoat.2007.01.044.

Aluservice, 2012. Aluservice - Product Catalogue, http://www.aluservice.com/pdf/Aluservice_21x21_2012_low_02.pdf.

ASM HandBook, 1994. ASM Metals HandBook Volume 5 - Surface Engineering. ASM HandBook.

Bononi, M., Conte, M., Giovanardi, R., Bozza, A., 2017. Hard anodizing of AA2099-T8 aluminum-lithium-copper alloy: Influence of electric cycle, electrolytic bath composition and temperature. Surface and Coatings Technology 325, 627–635. http://dx.doi.org/10.1016/j.surfcoat.2017.07.028.

BS EN 1706, 2020. Aluminium and aluminium alloys - Castings - Chemical composition and mechanical properties. BSI Standards Publication.

BS EN ISO 22557, 2020. Paints and varnishes – scratch test using a spring-loaded pen. bsi standards publication.

Caliari, D., 2017. Development and Optimization of Surface Hardening Treatments and Anodizing Processes. University of Padua, http://paduaresearch.cab.unipd.it/11040/1/TESI_Daniele_Caliari.pdf.

Chung, I.C., Chung, C.K., Su, Y.K., 2017. Effect of current density and concentration on microstructure and corrosion behavior of 6061 Al alloy in sulfuric acid. Surface and Coatings Technology 313, 299–306. http://dx.doi.org/10.1016/j.surfcoat.2017.01.114.

Chung, I.C., Chung, C.K., Su, Y.K., 2018. Effects of anodization parameters on the corrosion resistance of 6061 Al alloy using the Taguchi method. Microsystem Technologies 24 (1), 351–359. http://dx.doi.org/10.1007/s00542-017-3385-x.

Finger, C., Stiesch, M., Eisenburger, M., Breidenstein, B., Busemann, S., Greuling, A., 2020. Effect of sandblasting on the surface roughness and residual stress of 3Y-TZP (zirconia). SN Applied Sciences 2 (10), 1–8. http://dx.doi.org/10.1007/s42452-020-03492-6.

Fratila-Apachitei, L.E., Duszczyk, J., Katgerman, L., 2003. Vickers microhardness of AlSi(Cu) anodic oxide layers formed in H2SO4 at low temperature. Surface and Coatings Technology 165 (3), 309–315. http://dx.doi.org/10.1016/S0257-8972(02)00750-8.

Fratila-Apachitei, L.E., Terryn, H., Skeldon, P., Thompson, G.E., Duszczyk, J., Katgerman, L., 2004. Influence of substrate microstructure on the growth of anodic oxide layers. Electrochimica Acta 49 (7), 1127–1140. http://dx.doi.org/10.1016/j.electacta.2003.10.024.

Gastón-García, B., García-Lecina, E., Díaz-Fuentes, M., Díez, J.A., Müller, C., 2011. Sulphuric acid anodising of EN AC-46500 cast aluminium alloy. Transactions of the Institute of Metal Finishing 89 (6), 312–319. http://dx.doi.org/10.1179/174591911X13167804921037.

Henley, V.F., 1982. Anodic Oxidation of Aluminium and Its Alloys, first ed. Pergamin Press.

Kuo, J., 2014. Electron Microscopy - Methods and Protocols, third ed. Humana Press.

MIL-A-8625F, 1993. Military specification - Anodic coatings for aluminum and aluminum alloys.

Mohamed, A.M.A., Samuel, F.H., 2012. A review on the heat treatment of Al-Si-Cu/Mg casting alloys. In: Heat Treatment - Conventional and Novel Applications. http://dx.doi.org/10.5772/50282.

Mukhopadhyay, A.K., Sharma, A.K., 1997. Influence of Fe-bearing particles and nature of electrolyte on the hard anodizing behaviour of AA 7075 extrusion products. Surface and Coatings Technology 92 (3), 212–220. http://dx.doi.org/10.1016/S0257-8972(97)00102-3.

Niyazbakhsh, S., Amini, K., Gharavi, F., 2019. The effect of electrolyte temperature and sealing solution in anodizing operation on hardness and wear behavior of 7075-T6 aluminum alloy. Surface Review and Letters 26 (2), 1–7. http://dx.doi.org/10.1142/S0218625X18501433.

Poyner, J., 1991. Galvanoplastia - Electroplating Metal Anodizing Plating. Argus Books.

Poznyak, A., Pligovka, A., Laryn, T., Salerno, M., 2021. Porous alumina films fabricated by reduced temperature sulfuric acid anodizing: Morphology, composition and volumetric growth. Materials 14 (4), 1–16. http://dx.doi.org/10.3390/ma14040767.

Runge, J.M., 2018. The Metallurgy of Anodizing Aluminum, first ed. Springer, Cham.

Scampone, G., Timelli, G., 2022. Anodizing Al–Si foundry alloys: A critical review. Advanced Engineering Materials http://dx.doi.org/10.1002/adem.202101480.

Stojadinović, S., Vasilić, R., Kasalica, B., Belča, I., Zeković, L., 2014. Luminescence during the electrochemical oxidation of aluminum. pp. 241–302. http://dx.doi.org/10.1007/978-1-4939-0289-7_5.

Timelli, G., Fabrizi, A., 2014. The effects of microstructure heterogeneities and casting defects on the mechanical properties of high-pressure die-cast AlSi9Cu3(Fe) alloys. Metallurgical and Materials Transactions A: Physical Metallurgy and Materials Science 45 (12), 5486–5498. http://dx.doi.org/10.1007/s11661-014-2515-7.

Vandersluis, E., Ravindran, C., 2017. Comparison of measurement methods for secondary dendrite arm spacing. Metallography, Microstructure, and Analysis 6 (1), 89–94. http://dx.doi.org/10.1007/s13632-016-0331-8.

Vinal, G.W., Craig, D.N., 1934. Resistivity of sulphuric-acid solutions and its relation to viscosity and temperature. Journal of Research of the Rational Bureau of Standards 13, 689–697.

Zhu, B., Seifeddine, S., Jarfors, A.E.W., Leisner, P., Zanella, C., 2019. A study of anodising behaviour of Al-Si components produced by rheocasting. Solid State Phenomena 285 (SSP), 39–44. http://dx.doi.org/10.4028/www.scientific.net/SSP.285.39.

Zhu, B., Zanella, C., 2021. Influence of Fe-rich intermetallics and their segregation on anodising properties of Al-Si-Mg rheocast alloys. Surface and Coatings Technology 422, 127570. http://dx.doi.org/10.1016/j.surfcoat.2021.127570.